Robotica (2024), **42**, pp. 2388–2402
doi:10.1017/S0263574724000791

CAMBRIDGE UNIVERSITY PRESS

RESEARCH ARTICLE

A local collision-free motion planning strategy for hyper-redundant manipulators based on dynamic safety envelopes

Renjie Ju[1], Dong Zhang[1], Yan Gai[1] and Zhengcai Cao[2]

[1]College of Information Science and Technology, Beijing University of Chemical Technology, Beijing, China
[2]State Key Laboratory of Robotics and Systems, Harbin Institute of Technology, Harbin, China
Corresponding author: Zhengcai Cao; Email: caozc@hit.edu.cn

Received: 14 January 2024; **Revised:** 28 February 2024; **Accepted:** 16 April 2024; **First published online:** 12 September 2024

Keywords: hyper-redundant manipulator; obstacle avoidance; dynamic safety envelope; motion planning

Abstract

Hyper-redundant manipulators (HRMs) exhibit promising adaptability and superior dexterity in cavity detection tasks, owing to their snake-like segmented backbones. Due to the safety concern in contactless operating tasks, reliable motion planning in a confined environment for HRMs is very challenging. However, existing expanding-based obstacle avoidance methods are not feasible in narrow environments, as they will excessively occupy free spaces required for maneuvering. In this work, a local collision-free motion planning strategy based on dynamic safety envelope (DSE) is proposed for HRMs. First, the local motion of HRMs is analyzed in detail, and DSE is proposed for the first time to describe the boundary of the collision-free area. Then, to maximize the efficient utilization of narrow spaces, a reference trajectory for HRM is roughly planned without expanding obstacles. Further, a tip-guided trajectory tracking method based on configuration prediction is proposed by considering the discrete characteristics of rigid links to avoid obstacles. During the tracking process, DSEs are applied to evaluate collision risk and optimize the configuration. Finally, to validate the effectiveness of our proposed method, simulations are conducted, followed by experiments by using a 18-degrees of freedom mobile HRM prototype system.

1. Introduction

With advancements in robotics and automation, the capabilities to detect and maintain complex precision equipment have been significantly enhanced by a variety of specialized robots. These robots can effectively replace human beings in performing tasks that require narrow space operations [1–3]. Compared with conventional detection robots, hyper-redundant manipulators (HRMs) have better performances in diameter-to-length ratio, degrees of freedom (DOFs), and flexibility [4]. They provide a more efficient and noninvasive solution for contactless operating tasks, e.g., assembling in space station [5], maintaining pipelines in nuclear power plants [6], and detecting in deep cavity of huge equipment [7, 8].

Since the first HRM was proposed by Robinson in 1999 [9], various types of this robot have emerged in the past years. They can be roughly categorized in terms of their structures as a continuum type and the discrete one [10–12]. Despite continuum HRM features an infinite number of DOFs in theory, it is obviously impossible to activate all DOFs in practice. In contrast, the discrete one has higher accuracy and load capacity due to several rigid links and corresponding active revolute joints, which is more suitable for contactless operating tasks [13–15]. In our previous work, a cable-driven HRM with 16 independent DOFs was developed [16]. As shown in Fig. 1, the HRM is designed to inspect the narrow inner chamber of an aircraft engine.

© The Author(s), 2024. Published by Cambridge University Press.

https://doi.org/10.1017/S0263574724000791 Published online by Cambridge University Press

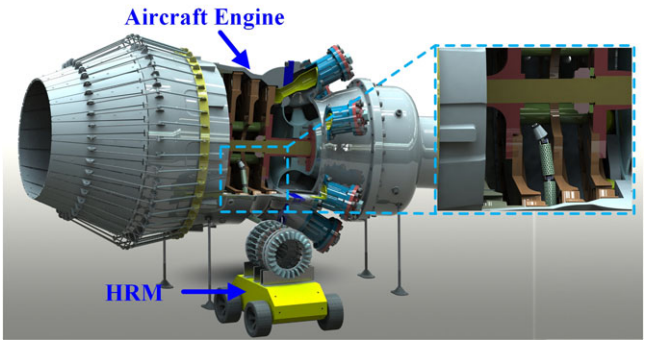

Figure 1. *Typical application scenario of HRM.*

Redundant DOFs cause significant influence on HRMs' dexterous control. Due to the strong nonlinearity and coupling constraints of HRMs, the motion planning and control of them pose significant challenges. Its core task is to find a collision-free trajectory under strictly environmental constraints. To solve it, various methods have been developed. In [17], Luo et al. propose a multiconstraint kinematic planning method based on variable redundancy kinematic model. They consider smoothness of joints and the mobility of base to obtain a collision-free path. Tian et al. [18] design an improved artificial potential field method for path planning. In it, by restricting the movement of the manipulators to a virtual guiding pipeline, the environmental adaptability of them in confined environments are improved. In ref. [19], an ellipsoid-shape rapidly exploring random tree method is proposed to plan a trajectory in a tunnel-like route. Zhang et al. [20] design an obstacle avoidance planning method based on the law of conservation of energy, which aims to ensure the smooth movement of the manipulator and avoid obstacles. Typically, expanded obstacles are commonly used to keep minimum safe distance in motion planning methods. However, in the process of expanding obstacles from their original size, there is a lack of established criteria for the expanded sizes. Each obstacle is uniformly expanded without distinction. Thus, these methods lack applicability in narrow deep cavities of aircraft engines.

In the domain of HRMs, various trajectory tracking control methods have been developed to make HRMs' shape fit their path curve. Wei et al. [21] present an autonomous motion planner with specialized rapidly exploring random tree for leader-following motion control of HRMs. In ref. [22], a decoupling control strategy for HRMs is proposed. The movements between their body and links are decoupled to perform fast full-link trajectory tracking under complex disturbances. Gill et al. [23] propose a frame curve-based method for path following control to determine the spline, which is currently closest to system outputs. Trajectory tracking-based motion planning methods have sufficient obstacle avoidance ability and high planning efficiency, which enhances the ability of HRMs to complete contactless operating tasks. Unfortunately, due to the discrete characteristic of HRM, it is not as flexible as the continuum robots. Thus, it is impossible to attain a perfect alignment with the path curve and only approximate trajectory tracking can be accomplished.

Despite the great progress of tracking-based motion planning methods, there is still a lack of consideration for potential collision areas during the tracking process. Besides, expanded obstacles may cause failed planning, especially in narrow environments. In this work, a local collision-free motion planning strategy based on dynamic safety envelope (DSE) is proposed. Its main contributions include:

- The structural characteristics and local motion of HRMs are analyzed. The DSE is proposed for the first time to describe the boundary of the potential collision area arising from approximate path tracking.
- In order to tackle the problem of excessive occupation of free space caused by expanded obstacles, the DSEs are applied to evaluate collision risks.
- Based on the designed HRM and the proposed DSE, a local collision-free motion planning strategy is proposed to guarantee the safety and efficiency of planning in confined environments.

https://doi.org/10.1017/S0263574724000791 Published online by Cambridge University Press

Table I. *Physical performance of HRM.*

Parameters	Values
Total DOFs	18
Motor numbers	26
Enveloped size of the manipulator (mm)	Φ 100 × 1375
Maximum speed of the wheeled platform (m/s)	0.8
Total mass (kg)	87.3
Load capability (kg)	0.5
Cable size (mm)	Φ 1

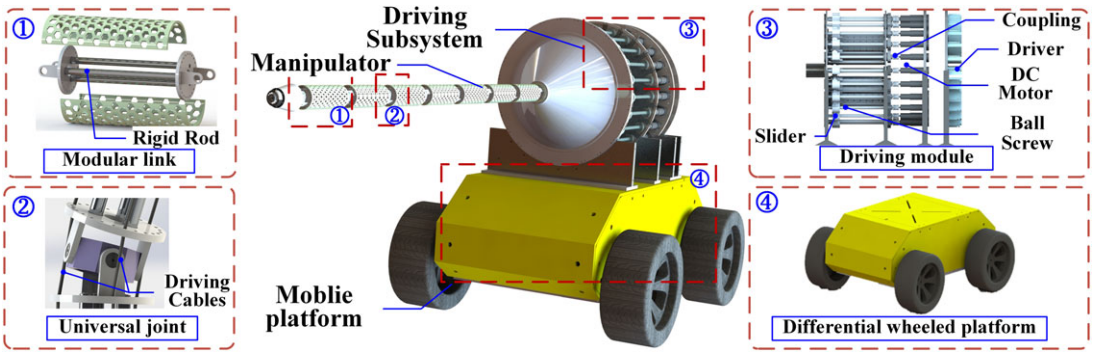

Figure 2. *Mechanism design of the proposed mobile HRM.*

The remainder of this paper is organized as follows. Section 2 details the mechanism design and kinematics of our HRM. The DSEs are proposed and analyzed in Section 3. Section 4 presents the local collision-free motion planning strategy based on DSEs. The simulations and experiments are conducted in Section 5. Finally, a conclusion is drawn in Section 6.

2. Mechanism descriptions and modeling of HRM

2.1. Mechanism design

Our previous work has demonstrated the motion performance of a manipulator [16]. In this work, our HRM is placed on a 2-DOFs wheeled platform to improve its wide-range mobility, as shown in Fig. 2. It is designed for delivering the robot tip to desired locations in aircraft engines by following the inner cavity. The main structure consists of a manipulator and a driving subsystem. The modular manipulator has 8 active universal joints with 16 rotational DOFs. It is driven by wire cables in order to provide accurate driving force and all driven cables are controlled by 24 driving modules. Each driving module is composed of a linear guide rail, slider, ball screw, coupling, DC motor, and motor driver. For faster installation and maintenance, the driving modules are arranged circularly. Its physical performances are listed in Table I.

2.2. Kinematics modeling

For motion planning of HRM in confined environments, it is crucial to obtain an accurate kinematics model. Based on the above mechanism design, the physical constraints are seriously considered. HRMs are usually modeled in the task, joint, and driving spaces. Respectively, their kinematics are further decomposed into two sub-kinematics as shown in Fig. 3.

https://doi.org/10.1017/S0263574724000791 Published online by Cambridge University Press

Table II. *POE parameters of HRM.*

Index	ω_i	q_i
1	$[0, 0, 1]^T$	$[0, 0, 0]^T$
2	$[0, -1, 0]^T$	$[0, 0, 0]^T$
3	$[0, -1, 0]^T$	$[d_l, 0, 0]^T$
4	$[0, 0, 1]^T$	$[d_l, 0, 0]^T$
⋮	⋮	⋮
15	$[0, -1, 0]^T$	$[7d_l, 0, 0]^T$
16	$[0, 0, 1]^T$	$[7d_l, 0, 0]^T$

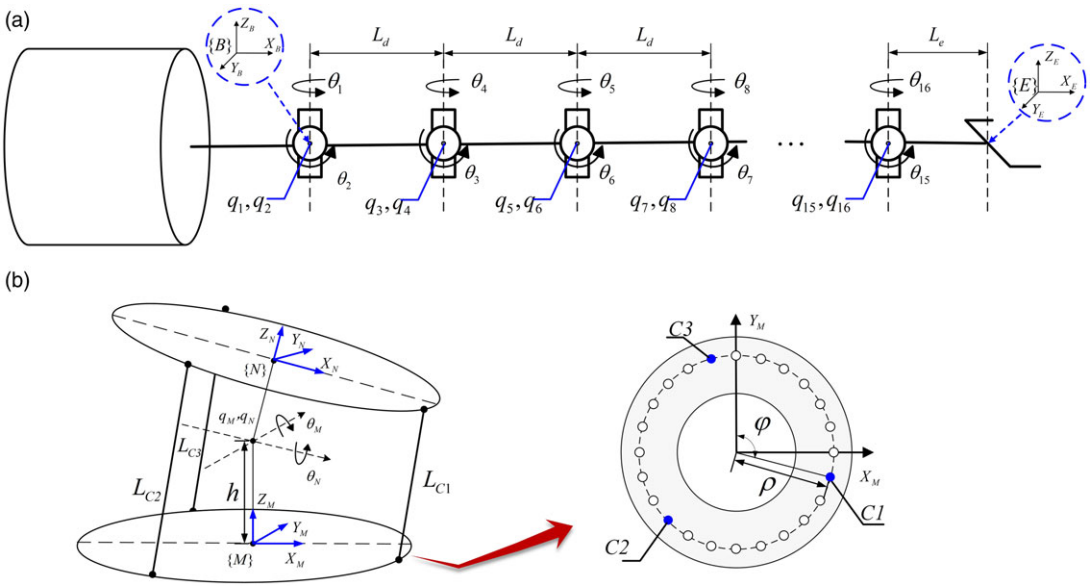

Figure 3. *Kinematics of: (a) the manipulator; (b) the driven cables.*

2.2.1. Kinematics of the manipulator

During the motion planning process of HRM, the current posture of the end-effector is calculated according to the rotational joints. In this work, product-of-exponential (POE) method is applied to describe the geometrical relations of HRM and avoid singularity solutions [24, 25]. As shown in Fig. 3(a), a base coordinate system B and an end coordinate system E are established.

POE parameters of the proposed HRM are listed in Table II, where ω_i is the unit direction vector of each axis, q_i represents the position of each joint. The motion of HRM can be described in the form of an exponential product as $e^{\hat{\xi}\theta}$. Therefore, its posture of HRM can be expressed as

$$f_1 = T_{B,E}(\theta_1, \theta_2, \theta_3, \ldots, \theta_{16}) = e^{\hat{\xi}_1\theta_1} e^{\hat{\xi}_2\theta_2} e^{\hat{\xi}_3\theta_3} \ldots e^{\hat{\xi}_{16}\theta_{16}} T_{B,E}(0), \tag{1}$$

where $T_{B,E}$ represents the transformation matrix from S to B and $\theta_1, \theta_2, \ldots, \theta_{16}$ are angles of rotational axes. The twist $\hat{\xi}_i = [\hat{\omega}_i, \nu_i; 0, 0]$, where $\hat{\omega}_i$ is the skew symmetric matrix of ω_i and $\nu_i = -\omega_i \times q_i$. Besides, $T_{B,E}(0)$ is the initial posture of HRM. In this work, the initial joint angles corresponding to initial state of HRM are set as $\theta_i = 0°$.

https://doi.org/10.1017/S0263574724000791 Published online by Cambridge University Press

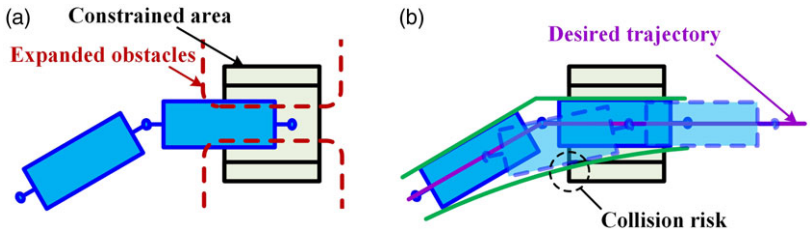

Figure 4. *Potential issues by using traditional methods during the trajectory tracking process: (a) excessive-expanded obstacles; (b) deviation from ideal trajectory.*

2.2.2. Kinematics of the driven cable

The main task in kinematics of the driven cable is to establish the mapping relationship between cable lengths and rotational joint angles. As shown in Fig. 3(b), a kinematic model is established to analyze the universal joint, and POE methods are applied to solve this problem. M and N are reference coordinate systems of two disks. The two rotational axes are intersect at the center of the universal joint. h represents the vertical distance between the disk and center of the universal joint. Further, the POE parameters are described by $\omega_M = [0,\ 1,\ 0]^T$, $\omega_N = [1,\ 0,\ 0]^T$, and $q_M = q_N = [0,\ 0,\ h]^T$. The initial posture of the joint is

$$T_{M,N}(0) = \begin{bmatrix} 1 & 0 & 0 & 0 \\ 0 & 1 & 0 & 0 \\ 0 & 0 & 1 & 2h \\ 0 & 1 & 0 & 1 \end{bmatrix}. \tag{2}$$

Then, the transformation matrix from M to N is

$$\begin{aligned} T_{M,N}(\theta_M, \theta_N) &= e^{\hat{\xi}_1 \theta_M} e^{\hat{\xi}_2 \theta_N} T_{M,N}(0) \\ &= \begin{bmatrix} \cos\theta_M & \sin\theta_M \sin\theta_N & \sin\theta_M \cos\theta_N & h \sin\theta_M \cos\theta_N \\ 0 & \cos\theta_N & -\sin\theta_N & -h \sin\theta_N \\ -\sin\theta_M & \cos\theta_M \sin\theta_N & \cos\theta_M \cos\theta_N & h + h\cos\theta_M \cos\theta_N \\ 0 & 0 & 0 & 1 \end{bmatrix}. \end{aligned} \tag{3}$$

The cable length L_{Ci} is the distance between the corresponding holes on disks, where i is the index of each cable. The position of cables in M is ${}^M C_i = \left[\rho\cos\varphi,\ \rho\sin\varphi,\ 0,\ 1\right]^T$, where ρ is the distance from cable hole to the center of disk. After that, the kinematic of driven cables can be obtained as

$$\begin{aligned} L_c(\theta_M, \theta_N, \varphi) &= \| T_{M,N}{}^N C_\varphi - {}^M C_\varphi \| \\ &= ((\rho\cos\varphi(\cos\theta_M - 1) + h\sin\theta_M \cos\theta_N + \rho\sin\varphi\sin\theta_M \sin\theta_N)^2 \\ &\quad + (\rho\sin\varphi(\cos\theta_N - 1) - h\sin\theta_N)^2 + (h(\cos\theta_M \cos\theta_N + 1) - \rho\cos\varphi\sin\theta_M \\ &\quad + \rho\sin\varphi\cos\theta_M \sin\theta_N)^2)^{\frac{1}{2}}. \end{aligned} \tag{4}$$

3. DSE-based collision detection method

As shown in Fig. 4(a), free space for maneuvering will be occupied by using traditional expanding-based methods. Excessive-expanded obstacles result in the failure of the planning process. Besides, due to the HRM cannot completely track the trajectory, area swept by rigid links during the tracking process needs to be researched. As shown in Fig. 4(b), HRMs deviate from the ideal trajectory, and collision risks may occur. However, in the presence of obstacles, there lacks detailed analysis related to this swept area. Therefore, the collision detection method based on DSE is proposed.

https://doi.org/10.1017/S0263574724000791 Published online by Cambridge University Press

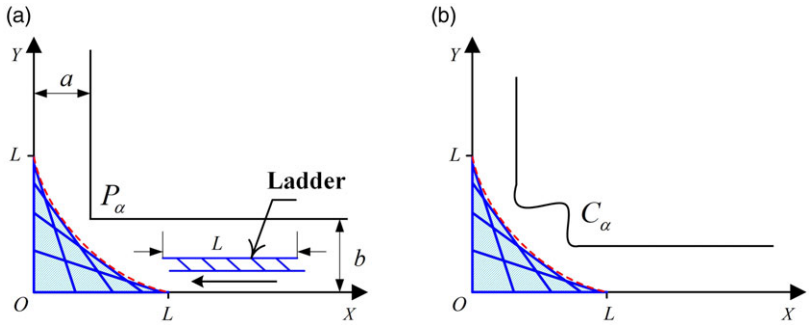

Figure 5. *Ladder problem with: (a) L-shaped corner; (b) irregular corner.*

3.1. Ladder problem

In order to provide a better understanding, the classical ladder problem is introduced first. As shown in Fig. 5(a), it can be described that how to operate a ladder to cross the L-shaped corner. In the idealized geometry, a line of constant length moves along the coordinate axes and forms a swept area. By definition, the envelope is a curve which is tangent at each of its points to the ladder. Interestingly, the envelope of this area is a part of a 4-cusped hypocycloid called astroid, with an equation in Cartesian coordinates:

$$x^{\frac{2}{3}} + y^{\frac{2}{3}} = L^{\frac{2}{3}}, \tag{5}$$

where L is the length of the ladder [26]. In order for the ladder to pass through the corner without collision, the corner point $P_\alpha(a, b)$ needs to be outside the envelope and satisfy $a^{\frac{2}{3}} + b^{\frac{2}{3}} > L^{\frac{2}{3}}$.

Further discussion of the ladder problem is illustrated in Figure 5(b), where the L-shaped corner is replaced by an irregular corner. Accordingly, we assume that the irregular corner is formed by curve C_α, and (x_α, y_α) is a point of C_α. To avoid collisions, (x_α, y_α) needs to satisfy $x_\alpha{}^{\frac{2}{3}} + y_\alpha{}^{\frac{2}{3}} > L^{\frac{2}{3}}$.

Similarly, collision risks occur where the trajectory is curved tightly during the tracking process of HRM. Inspired by the ladder problem, the potential collision area C_p is defined as is the interior of the swept area. DSE is defined as the inner boundary curve of C_p. The main properties of C_p are

- C_p usually occurs on the concave side of the trajectory.
- When the curvature of trajectory tends to be infinitesimal, which means the trajectory tends to a straight line, the area of C_p tends to be infinitesimal.

3.2. Parameterization of DSE

An extended variation on the above ladder problem is shown in Fig. 6. When the tracking trajectory is no longer vertical, the other side of the ladder P_{i+1} moves on any line passing through the origin of coordinates. α is the angle between the line and the horizontal axis.

To facilitate the calculation, the $X'OY'$ coordinate system is established with $\angle X'OX = \frac{\alpha}{2}$. In XOY coordinate system, we assume that $P_i(u, 0)$,P_{i+1} $(v\cos\alpha, v\sin\alpha)$, where $u \in [-1, 0]$ and $v \in [0, 1]$. Then, in $X'OY'$ coordinate system, we have $P'_i\left(u\cos\frac{\alpha}{2}, -u\sin\frac{\alpha}{2}\right)$,$P'_{i+1}\left(v\cos\frac{\alpha}{2}, v\sin\frac{\alpha}{2}\right)$. L_d is the length of $P'_iP'_{i+1}$. In the derivation process, we assume that $L_d = 1$. $G(x', y', v)$ is defined as a family of lines with parameters u and v. According to $P'_iP'_{i+1}$, it can be obtained:

$$G(x', y', v) = \frac{y' + u\sin\dfrac{\alpha}{2}}{v\sin\dfrac{\alpha}{2} + u\sin\dfrac{\alpha}{2}} - \frac{x' - u\cos\dfrac{\alpha}{2}}{v\cos\dfrac{\alpha}{2} - u\cos\dfrac{\alpha}{2}}. \tag{6}$$

By the cosine theorem in $\Delta P'_iOP'_{i+1}$, u and v linked by the relation $(u+v)^2 = 1 + 4uv\cos^2\frac{\alpha}{2}$.

https://doi.org/10.1017/S0263574724000791 Published online by Cambridge University Press

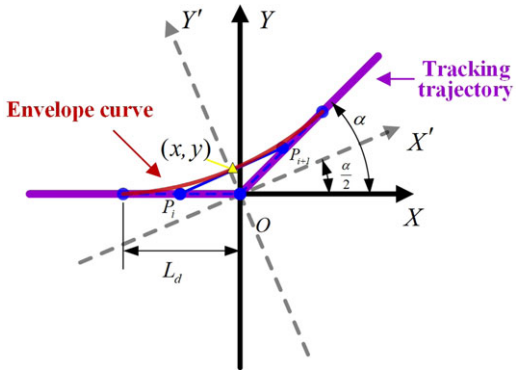

Figure 6. *Illustration of geometric approach for DSE.*

In general, the DSE can be obtained:

$$G(x', y', v) = 0,$$
$$\frac{\partial G(x', y', v)}{\partial v} = 0. \tag{7}$$

It represents that an envelope of the family $G(x', y', v)$ is a curve that is tangent to each member of the family at some point. By combining (6) and (7), the envelope in $X'OY'$ coordinate system is

$$\begin{cases} x' = L_d(v+u)\cos\dfrac{\alpha}{2}\left(1 - 2uv\sin^2\dfrac{\alpha}{2}\right), \\ y' = L_d(v-u)\sin\dfrac{\alpha}{2}\left(1 + 2uv\cos^2\dfrac{\alpha}{2}\right). \end{cases} \tag{8}$$

Therefore, the corresponding envelope in XOY coordinate system can be obtained in the form:

$$\begin{cases} x = L_d v\cos\alpha + \dfrac{1}{2}L_d u(2 - v^2 + v^2\cos 2\alpha), \\ y = L_d v(1 - u^2 + uv\cos\alpha)\sin\alpha. \end{cases} \tag{9}$$

As shown in Fig. 7(a), E_1-E_4 are envelope curves, and the potential collision area C_p tends to be infinitesimal when α tend to be 0°. It indicates that as deflection angle of the trajectory increases, the collision risk of HRM increases correspondingly. Figure 7(b) illustrates the positive correlations between C_p and L_d, which means the geometric parameters of the HRM are crucial in its ability to navigate through obstacles. Further, the potential collision area C_p is formed by multiple envelope curves E_1-E_4 in case of multisegment trajectories as shown in Fig. 7(c). Especially, if the trajectory is a continuous arc as shown in Fig. 7(d), C_p can be formed by overlaying the envelopes of multiple discrete trajectories. By parameterizing the DSE, multisegment HRM can effectively avoid collision-risk areas.

3.3. DSEs considering the geometric dimensions of HRM

The authenticity of the scenario is enhanced by recognizing that the HRM actually has some positive width. As shown in Fig. 8, the centerline of HRM's link is aligned with the tracking trajectory, which forms an original safety envelope E_1. Similarly, an envelope E_2 occurs by the H family, which consists of line segments separated from G family by width d_w. The parameterized representation of E_1 has been derived above, and the relationships between E_1 and E_2 are obtained in this part.

In $X'OY'$ coordinate system, lines of G family are described in (6), which can be rewrote as

$$G(x', y', v) = (u+v)\sin\frac{\alpha}{2}x' + (u-v)\cos\frac{\alpha}{2}y' - uv\sin\frac{\alpha}{2}, \tag{10}$$

https://doi.org/10.1017/S0263574724000791 Published online by Cambridge University Press

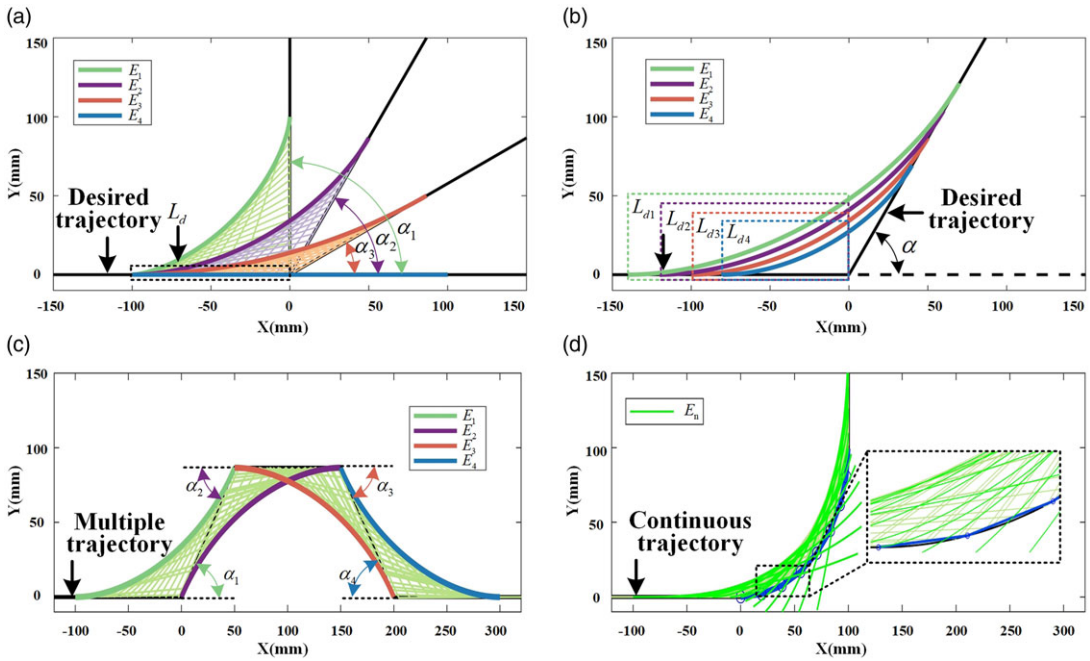

Figure 7. *Related properties of DSEs: (a) change α under constant L_d; (b) change L_d under constant α; (c) envelope curves of multisegment trajectories; (d) envelope curves of continuous trajectory.*

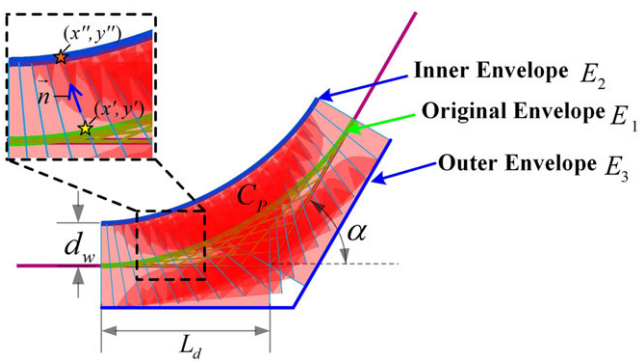

Figure 8. *DSEs generated by actual cylindrical link.*

where

$$\left((u+v)\sin\frac{\alpha}{2}\right)^2+\left((u-v)\cos\frac{\alpha}{2}\right)^2=1. \tag{11}$$

The normal unit vector of G is defined as

$$\overrightarrow{n}=\left((u+v)\sin\frac{\alpha}{2},(u-v)\cos\frac{\alpha}{2}\right). \tag{12}$$

To be convenient, the functions can be expressed as

$$\begin{aligned} G(x',y',v)&=\overrightarrow{n}\cdot(x',y')-uv\sin\alpha,\\ H(x',y',v)&=\overrightarrow{n}\cdot(x',y')-uv\sin\alpha-d_w, \end{aligned} \tag{13}$$

https://doi.org/10.1017/S0263574724000791 Published online by Cambridge University Press

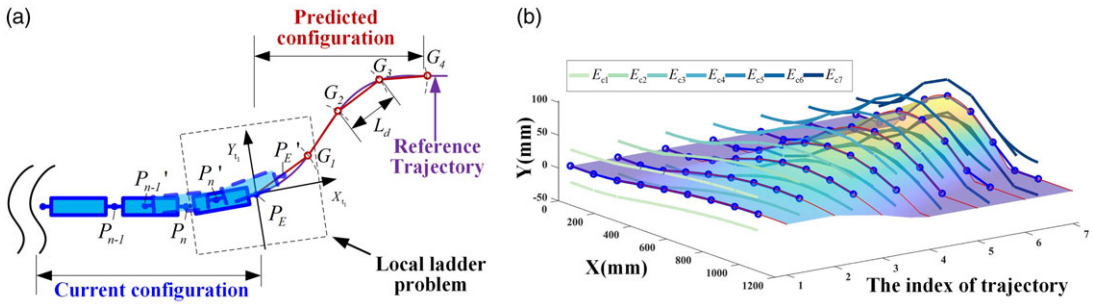

Figure 9. *The configuration prediction method: (a) Illustration of the method; (b) prediction results of different reference trajectories.*

Considering that (x', y') is on the envelope of G family, (x'', y'') is the corresponding point that is d_w units away in the normal direction. Thus, the H family is

$$\begin{aligned} H(x'', y'', v) &= \overrightarrow{n} \cdot (x'', y'') - uv \sin\alpha - d_w \\ &= \overrightarrow{n} \cdot [(x', y') + d_w \overrightarrow{n}] - uv \sin\alpha - d_w \\ &= G(x', y', v). \end{aligned} \tag{14}$$

Similarly, the partial derivative with respect to v is computed as $\frac{\partial H(x'', y'', v)}{\partial v} = \frac{\partial G(x', y', v)}{\partial v}$. The results show that if H family consists of parallel lines in G family separated by width d_w, the envelope E_2 is the parallel of E_1. In addition, E_3 is defined as the outer safety envelope. Obviously, it is parallel to the reference trajectory. Considering the geometric dimension, the ladder problem is transformed into couch problem. Indeed, as for the couch problem, the DSE and one of its parallel curves are applied to make it more in line with the actual situation of HRM. C_p is defined as the potential collision area formed by the inner safety envelope E_2 and the outer safety envelope E_3. In case of multiple obstacles $O_n = \bigcap_{i=1}^{n} O_i$, where n is the number of obstacles, the collision avoidance conditions can be expressed as $\left\{C_p \bigcap O_n = \emptyset\right\}$. In fact, evaluating potential collision areas rather than expanded obstacles gives more permissible space for motion planning.

4. Local collision-free motion planning strategy

Typically, deep cavities of an aircraft engine are more narrow and confined than normal environments, where more precise obstacle avoidance strategies are needed. Based on the designed HRM and the proposed DSE, a local collision-free motion planning strategy is proposed in detail. The motion planning of the HRM mainly includes two steps: a) configuration prediction, followed by b) configuration update. In the following, each module of the approach is described in detail.

4.1. Configuration prediction

To avoid failure planning results caused by over occupation of free space, the links' collision volumes and potential collision area are not considered during the planning process. With the reference trajectory, the traditional tracking method is to fit its link to the desired curve. However, it is difficult to give the mathematical expression of continuous curve, which may cause more computation time. To fully utilize the potential of the DSE, a configuration switching-based planning strategy is first proposed by discretizing motion process. Different with the real-time link fitting method, our approach is to directly predict future configurations of the HRM.

In order to provide the reader with a better understanding of the proposed method, a detailed illustration is given as shown in Fig. 9(a). The main idea of this method is tip-guided motion, which means that

https://doi.org/10.1017/S0263574724000791 Published online by Cambridge University Press

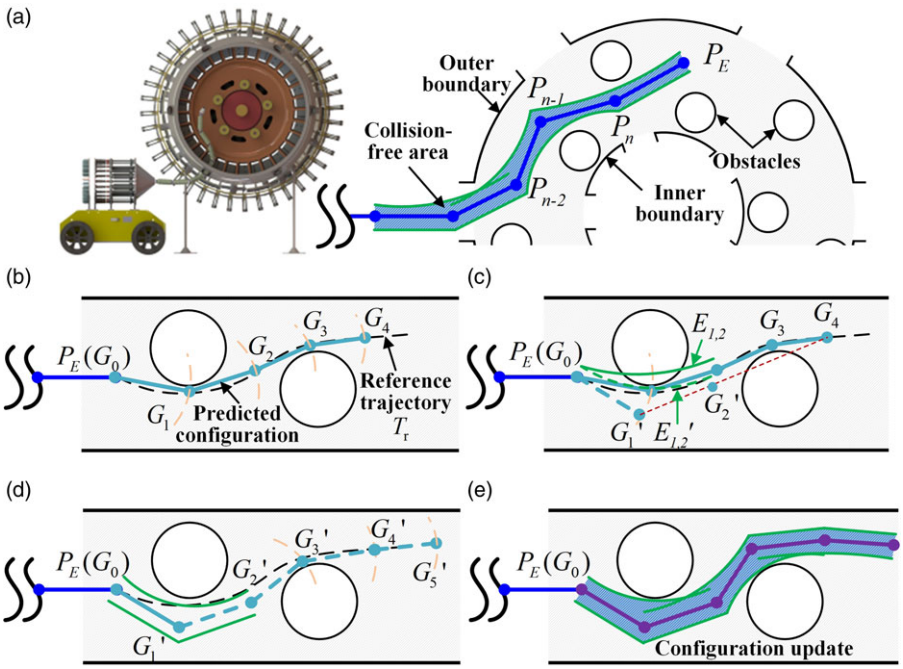

Figure 10. *The configuration update method of the HRM: (a) modeling of the internal environment of aircraft engine; (b) predicted configuration under the reference trajectory; (c) calculating DSEs and updating G_1', G_2'; (d) updating G_3', G_4' and predicting G_5'; (e) update result of collision-free configuration.*

only the motion of the last two links is considered. $P_{n-1}P_n$ and P_nP_E represent the current configuration of the last two links. To track the reference trajectory, the first step is to predict the next configuration of HRM. The statement of the problem is

$$\begin{aligned} \min_{G_i} \quad & \|G_i - P_t\|, \\ s.t. \quad & \|G_i - G_{i-1}\| - L_d = 0, \\ & G_i \in C_{ref}, G_0 = P_E \\ & i = 1, 2, 3, \cdots, n_j, \end{aligned} \tag{15}$$

where C_{ref} is the curve of the reference trajectory and G_i is the point on C_{ref}. Once the position of P_E is determined, the next n_j key nodes can be obtained. The distance between each two nodes is equal to the length of HRM's link, which means that the future configuration can be predicted.

It's worth noting that in the process of link P_nP_E transfer to P_EG_1, joint P_n' is on P_nP_E and joint P_E' is on P_EG_1. As mentioned in Section 3, it can be regarded as a local ladder problem with collision volume constraints. With the application of the DSE, the regions swept by the head links can be parameterized. Further, configuration prediction results are obtained from different reference trajectories as shown in Fig. 9(b). $E_{c1}, E_{c2}, \ldots, E_{c7}$ are envelope curves of them.

4.2. Configuration update

After predicting the configuration, it is necessary to update the configuration according to the obstacle situation. As shown in Fig. 10(a), the main task for HRM is to keep the manipulator moving within intracavity without colliding with local obstacles. The whole DSE-based configuration update method for HRM is shown in Algorithm 1.

https://doi.org/10.1017/S0263574724000791 Published online by Cambridge University Press

Algorithm 1 The DSE-based configuration update algorithm.

Input: Reference trajectory T_r, position of exist obstacles P_o, end position P_E, joint positions $P_1, P_2, ...P_n$, target position P_t, the maximum iterations T, distance threshold D

Output: Updated position of predicted configuration $G_0, G_1, ...G_k$

Initialize the number of successful step $i = 0$;
The distance between end-effector and target $d_{et} = \left|\overrightarrow{P_E P_t}\right|$;
while $d_{et} < D$ **do**
  $t = 0$;
  Predict configuration and obtain $G_i, G_{i+1}, ..., G_{i+4}$ via (15);
  Generate envelope of G_i, G_{i+1}, G_{i+2} via (9)–(14);
  Check collision risk from E and P_o;
  if *There exists collision risk* **then**
    while $t < T$ **do**
      Obtain the index of nearby obstacles P_o;
      Update G_{i+1} by joint rotation $\delta\theta$ in the direction away from the obstacle with L_d as the radius of rotation;
      $G_{i+2} = \left(1 - \frac{L_d}{\left|\overrightarrow{G_{i+1}G_{i+4}}\right|}\right) G_{i+1} + \frac{L_d}{\left|\overrightarrow{G_{i+1}G_{i+4}}\right|} G_{i+4}$;
      Recheck collision risk;
      $t = t + 1$;
    end
  end
  Update $G_i, G_{i+1}, G_{i+2}, d_{et}$;
  $i = i + 1$;
end
Return $G_0, G_1, ...G_k$.

First, the desired configuration is predicted and $G_0, G_1, \ldots, G_4$ are obtained via (15) as shown in Figure 10(b). G_0 coincides with point P_E. G_1, G_2, G_3, G_4 are located on the reference trajectory T_r and satisfy the distance constraints. Then, the envelope $E_{1,2}$ is calculated by considering G_0, G_1, G_2 as shown in Fig. 10(c). Obviously, $E_{1,2}$ is found in contact with the obstacle nearby. By fixing G_0, G_1 is rotated by angle $\delta\theta$ in the direction away from the obstacle with L_d as the radius of rotation where $\delta\theta$ represents the incremental angle for each iteration. Since our approach involves local updates, G_2 cannot deviate too far from the reference trajectory. After obtaining G_1', G_2' is planned on $G_1'G_4$ and calculated as

$$G_2' = \left(1 - \frac{L_d}{\left|\overrightarrow{G_1'G_4}\right|}\right) G_1' + \frac{L_d}{\left|\overrightarrow{G_1'G_4}\right|} G_4. \tag{16}$$

The next step is to recalculate the envelope and assess collision risk according to G_0, G_1', G_2'. As shown in Fig. 10(d), the above steps are repeated until there exists no collision risks. G_3', G_4', and G_5' are predicted in the same way via (15). After a step-by-step optimization, a collision-free configuration within narrow aircraft engine can finally be obtained, as shown in Fig. 10(e). In the above example, the calculation of G_0, G_1, G_2 and the evaluation of collision are the key to our method. G_3 and G_4 are thoughtfully crafted to make the most of the reference trajectory T_r, ensuring that all subsequent points are smoothly updated toward the ultimate goal.

It should be emphasized that the advantage of our strategy lies in the utilization of confined space. The geometric dimensions of HRM's links and potential collision areas are considered in the envelope

https://doi.org/10.1017/S0263574724000791 Published online by Cambridge University Press

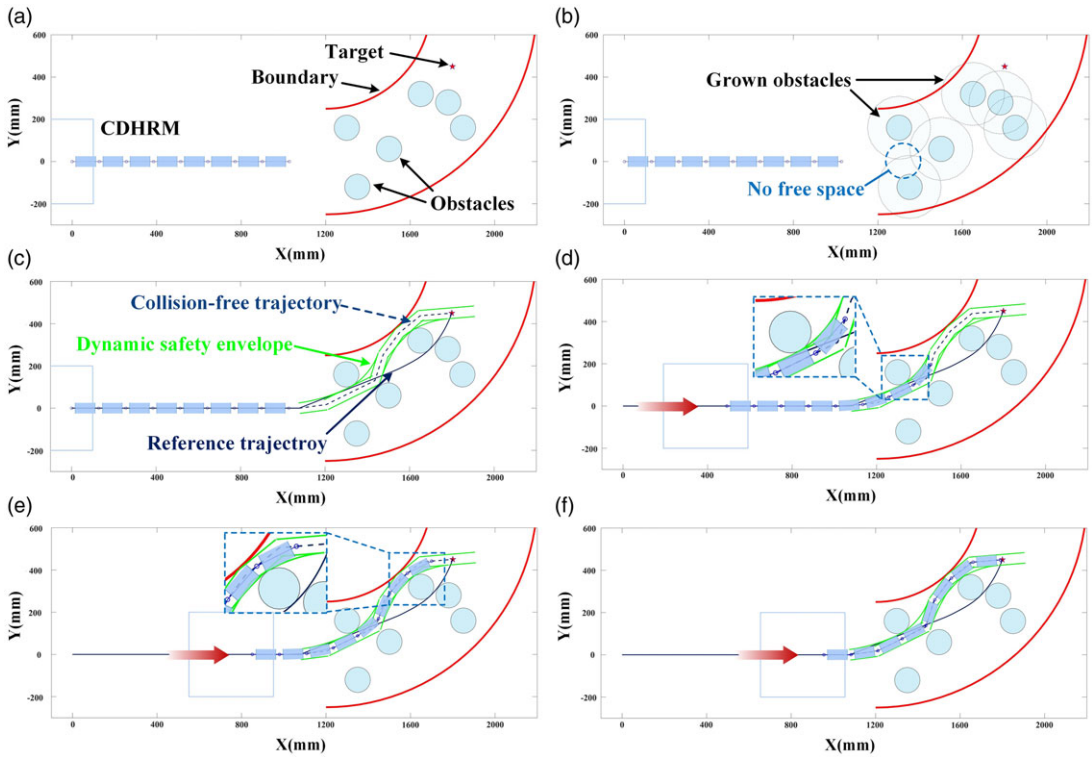

Figure 11. *Simulation of HRM in narrow environment by the proposed method.*

calculation process. On this base, the links are simplified into length-fixed segments, and obstacles are maintained in their original size.

5. Simulation and experimental validation

5.1. Simulations of HRM in narrow environments

In order to verify the proposed methods, simulations are implemented. This serves to illustrate the unique advantage of DSEs in motion planning. All of the numerical simulations are performed on a PC with an AMD Ryzen 7 3700X 8-Core Processor 3.60 GHz and 16-GB memory.

As shown in Fig. 11(a), the virtual model of an aircraft engine and a mobile HRM are established. The initial configuration of HRM is set to horizontal. The length of each rigid link L_d is set to 128.5mm, the same size as the actual robot. The red arcs indicate the inner and outer boundary of the aircraft engine, and the distance between these boundaries is set to 500mm. The obstacles are tightly arranged within two boundaries and the radius of each obstacle is 60mm. In compact part, narrow gaps are set for HRM to pass through. The common method of expanded obstacles is shown in Fig. 11(b). To ensure the safety of planning, the link width d_w and the potential collision areas are considered to calculate the expanded size of obstacles. In this work, $d_w = 25mm$. According to (9) and (14), the maximum safety expanded size is set to 89.25mm where the path deflection angle $\alpha = 90°$. However, expanded areas excessively occupy narrow spaces, and there exists no free space for the HRM to obtain a proper trajectory.

The result of proposed method based on DSEs is shown in Fig. 11(c). The reference trajectory is obtained by the combination of an artificial bee colony algorithm and a particle swarm optimization algorithm [27]. The DSE is calculated, and the collision-free trajectory is obtained by our strategy. Figs. 11(d)-(f) show the trajectory tracking results during the movement of HRM.

https://doi.org/10.1017/S0263574724000791 Published online by Cambridge University Press

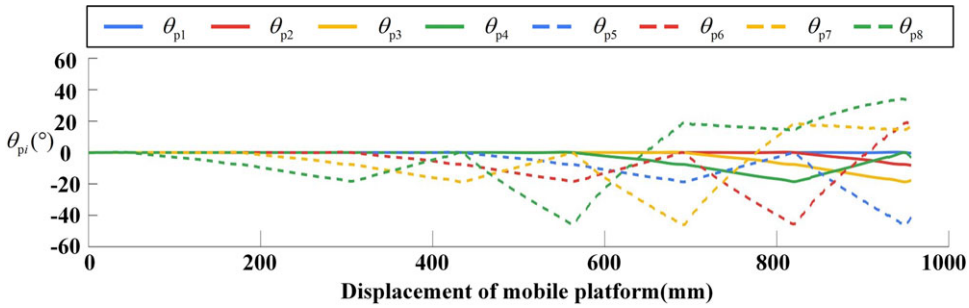

Figure 12. *Pitch rotation joint angles of simulation.*

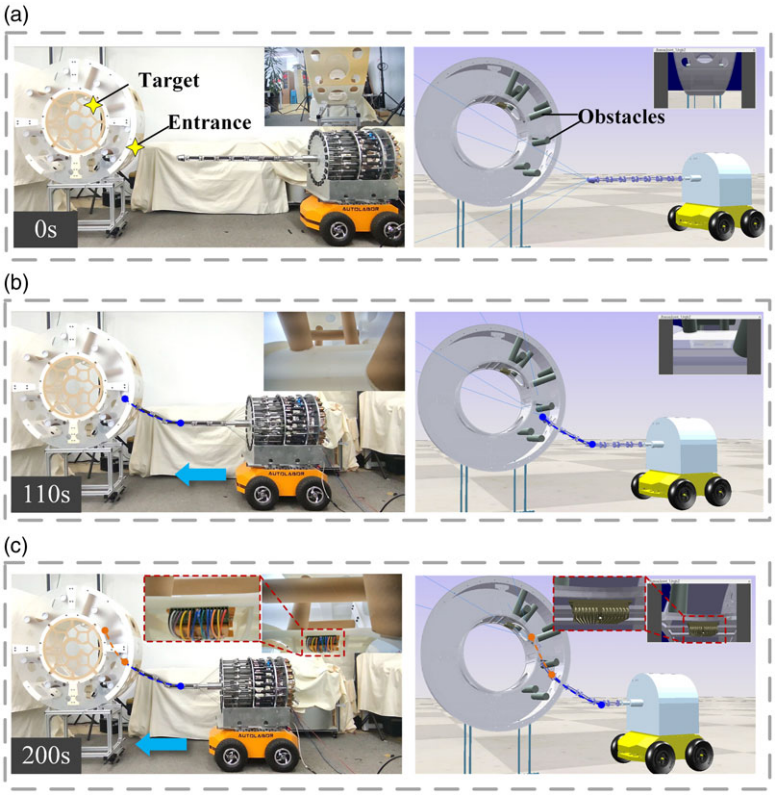

Figure 13. *Experiments of intracavity exploration by the proposed method.*

As shown in Fig. 12, the pitch rotation joint angles $\theta_{p1}, \theta_{p2}, \ldots, \theta p8$ are solved. $\theta p8$ represents the end pitch rotation joint angle. Due to the tip-guided trajectory tracking method, the rest joints are followed sequentially by the end joint. The simulations indicate that the proposed strategy enable HRM to precisely avoid obstacles in confined aircraft engines.

5.2. Experiments of intracavity exploration

In this part, experimental validation is conducted on an actual HRM system to verify the adaptability of our strategy as shown in Fig. 13(a). In order to accomplish detection tasks in aircraft engine, an annular cavity is constructed first. The same virtual model is built in COPPELIASIM, as shown in the right part of Fig. 13(a). The HRM is supposed to cross a narrow space and reach the faulty electronic component to conduct detection tasks. In this experiment, the initial joint angles corresponding to initial state of

https://doi.org/10.1017/S0263574724000791 Published online by Cambridge University Press

HRM are set to $\theta_i = 0°$. Figs. 13(a)-(c) are current motion images of HRM move into obstacle array at $t = 0$s, 110s, and 200s, respectively. It is concluded that the proposed strategy makes HRM to avoid obstacles and reach the target point accurately.

6. Conclusion

Driven by the safety concern in contactless operating tasks, a local collision-free motion planning strategy is proposed for HRMs based on DSE. For the method, the tracking processes of HRMs are analyzed in detail, and the concept of DSE is first proposed to describe the boundary of the collision-free area. In order to guarantee the efficiency of motion planning in confined environments, trajectory of HRM's end-effector is roughly planned without expanded obstacles. Further, the DSEs are applied to evaluate collision risk and optimize the trajectory in real time. Performances of our strategy are verified by simulations and experiments. Advantage of the DSE in the motion planning of HRMs is demonstrated.

Our strategy proposed in this work expands the potential of HRM in maintenance of narrow aircraft engines. Our future work includes dynamic modeling, energy optimization, and precise motion control of HRMs [28–31]. The DSE can be extended to three-dimensional space. Furthermore, intelligent optimization and other advanced methods should be applied to improve the performance of HRMs [32, 33].

Author contributions. Renjie Ju, Dong Zhang, Yan Gai, and Zhengcai Cao conceived and designed the study and wrote the article.

Financial support. This work was supported by the Beijing Natural Science Foundation (L223019, 3242011) and National Natural Science Foundation of China (52105005).

Competing interests. The authors declare no competing interests exist.

Ethical approval. The authors declare none.

References

[1] X. Dong, M. Wang, A. Mohammad, W. Ba, M. Russo, A. Norton, J. Kell and D. Axinte, "Continuum robots collaborate for safe manipulation of high-temperature flame to enable repairs in challenging environments," *IEEE/ASME Trans Mechatro* **27**(5), 4217–4220 (2022).

[2] Z. Mu, L. Zhang, L. Yan, Z. Li, R. Dong, C. Wang and N. Ding, "Hyper-redundant manipulators for operations in confined space: Typical applications, key technologies, and grand challenges," *IEEE Trans Aero Elec Syst* **58**(6), 4928–4937 (2022).

[3] Z. Ji, G. Song, F. Wang, Y. Li and A. Song, "Design and control of a snake robot with a gripper for inspection and maintenance in narrow spaces," *IEEE Robot Autom Lett* **8**(5), 3086–3093 (2023).

[4] I. Walker, H. Choset and G. Chirikjian, *Snake-Like and Continuum Robots* (Springer Handbook of Robotics, 2016).

[5] Z. Mu, T. Liu, W. Xu, Y. Lou and B. Liang, "Dynamic feedforward control of spatial cable-driven hyper-redundant manipulators for on-orbit servicing," *Robotica* **37**(1), 18–38 (2019).

[6] R. Buckingham and A. Graham, "Dexterous Manipulators for Nuclear Inspection and Maintenance-Case Study," **In:** *IEEE International Conference on Applied Robotics for the Power Industry*, (2010) pp. 1–6.

[7] M. Hwang and D-S Kwon, "K-flex: A flexible robotic platform for scar-free endoscopic surgery," *Int J Med Robot Comput Assi Surg* **16**(2), e2078 (2020).

[8] C. Lauretti, T. Grasso, E. de Marchi, S. Grazioso and G. di Gironimo, "A geometric approach to inverse kinematics of hyper-redundant manipulators for tokamaks maintenance," *Mech Mach Theory* **176**, 104967 (2022).

[9] G. Robinson and J. B. C. Davies, "Continuum Robots - A State of the Art," **In:** *IEEE International Conference on Robotics and Automation*, (1999) pp. 2849–2854.

[10] R. Kang, Y. Guo, L. Chen, D. Branson and J. Dai, "Design of a pneumatic muscle based continuum robot with embedded tendons," *IEEE/ASME Trans Mechatro* **22**(2), 751–761 (2017).

[11] C. Yang, S. Geng, I. Walker, D. T. Branson, J. Liu, J. S. Dai and R. Kang, "Geometric constraint-based modeling and analysis of a novel continuum robot with shape memory alloy initiated variable stiffness," *Int J Robot Res* **39**(14), 1620–1634 (2020).

[12] J. Kim, S.-I. Kwon, Y. Moon and K. Kim, "Cable-movable rolling joint to expand workspace under high external load in a hyper-redundant manipulator," *IEEE/ASME Trans Mechatro* **27**(1), 501–512 (2022).

https://doi.org/10.1017/S0263574724000791 Published online by Cambridge University Press

[13] T. Liu, W. Xu, T. Yang and Y. Li, "A hybrid active and passive cable-driven segmented redundant manipulator: Design, kinematics, and planning," *IEEE/ASME Trans Mechatro* **26**(2), 930–942 (2021).
[14] A. Martín-Barrio, J. J. Roldán-Gómez, I. Rodríguez, J. del Cerro and A. Barrientos, "Design of a hyper-redundant robot and teleoperation using mixed reality for inspection tasks," *Sensors* **20**(8), 2181 (2020).
[15] Z. Cao, D. Zhang and M. C. Zhou, "Direction control and adaptive path following of 3-d snake-like robot motion," *IEEE Trans Cybern* **52**(10), 10980–10987 (2022).
[16] R. Ju, D. Zhang, J. Xu, H. Yuan, Z. Miao, M. Zhou and Z. Cao, "Design, modeling, and kinematics analysis of a modular cable-driven manipulator," *ASME J Mech Robot* **14**(6), 060903 (2022).
[17] M. Luo, E. Li, A. Zhang, M. Tan and Z. Liang, "A bioinspired coiled cable-driven manipulator: Mechatronic design and kinematics planning with multiconstraints," *IEEE/ASME Trans Mechatro* **28**(6), 3155–3166 (2023).
[18] Y. Tian, X. Zhu, D. Meng, X. Wang and B. Liang, "An overall configuration planning method of continuum hyper-redundant manipulators based on improved artificial potential field method," *IEEE Robot Autom Lett* **6**(3), 4867–4874 (2021).
[19] H. Ji, H. Xie, C. Wang and H. Yang, "E-RRT∗: Path planning for hyper-redundant manipulators," *IEEE Robot Autom Lett* **8**(12), 8128–8135 (2023).
[20] H. Zhang, H. Jin, Z. Liu, Y. Liu, Y. Zhu and J. Zhao, "Real-time kinematic control for redundant manipulators in a time-varying environment: Multiple-dynamic obstacle avoidance and fast tracking of a moving object," *IEEE Trans Ind Inform* **16**(1), 28–41 (2020).
[21] H. Wei, Y. Zheng and G. Gu, "Rrt-Based Path Planning for Follow-the-Leader Motion of Hyper-Redundant Manipulators," **In:** *IEEE/RSJ International Conference on Intelligent Robots and Systems*, (2021) pp. 3198–3204.
[22] X. Jiang, F. Yang and S. Shi, "Design and full-link trajectory tracking control of underwater snake robot with vector thrusters under strong time-varying disturbances," *Ocean Eng* **266**(3), 113012 (2022).
[23] R. J. Gill, D. Kulic and C. Nielsen, "Spline path following for redundant mechanical systems," *IEEE Trans Robot* **31**(6), 1378–1392 (2015).
[24] C. Li, Y. Wu, H. Lowe and Z. Li, "Poe-based robot kinematic calibration using axis configuration space and the adjoint error model," *IEEE Trans Robot* **32**(5), 1264–1279 (2016).
[25] C. Yang, R. Kang, D. T. Branson, L. Chen and J. S. Dai, "Kinematics and statics of eccentric soft bending actuators with external payloads," *Mech Mach Theory* **139**, 526–541 (2019).
[26] T. Dana-Picard, "An automated study of isoptic curves of an astroid," *J Symb Comput* **97**, 56–68 (2020).
[27] Z. Li, W. Wang, Y. Yan and Z. Li, "PS–ABC: A hybrid algorithm based on particle swarm and artificial bee colony for high-dimensional optimization problems," *Expert Syst Appl* **42**(22), 8881–8895 (2015).
[28] F. Aimedee, G. Gogu, J. S. Dai, C. Bouzgarrou and N. Bouton, "Systematization of morphing in reconfigurable mechanisms," *Mech Mach Theory* **96**, 215–224 (2016).
[29] Z. Cao, J. Li, D. Zhang, M. Zhou and A. Abusorrah, "A multi-object tracking algorithm with center-based feature extraction and occlusion handling," *IEEE Trans Intell Transp Syst* **24**(4), 4464–4473 (2022).
[30] T. Sun, S. Yang, T. Huang and J. S. Dai, "A way of relating instantaneous and finite screws based on the screw triangle product," *Mech Mach Theory* **108**, 75–82 (2017).
[31] Z. Cao, Q. Xiao and M. Zhou, "Distributed fusion-based policy search for fast robot locomotion learning," *IEEE Comput Intell Mag* **14**(3), 19–28 (2019).
[32] C. R. Lin, Z. C. Cao and M. C. Zhou, "Learning-based cuckoo search algorithm to schedule a flexible job shop with sequencing flexibility," *IEEE Trans Cybernetics* **53**(10), 6663–6675 (2023).
[33] J. Li, D. Li, C. Wang, W. Guo, Z. Wang, Z. Zhang and H. Liu, "Active collision avoidance for teleoperated multi-segment continuum robots toward minimally invasive surgery," *Int J Robot Res* **43**(7), 918–941. (2024).

Cite this article: R. Ju, D. Zhang, Y. Gai and Z. Cao (2024). "A local collision-free motion planning strategy for hyper-redundant manipulators based on dynamic safety envelopes", Robotica **42**, 2388–2402. https://doi.org/10.1017/S0263574724000791

https://doi.org/10.1017/S0263574724000791 Published online by Cambridge University Press